IEEE Access
Multidisciplinary | Rapid Review | Open Access Journal

Received October 9, 2018, accepted October 25, 2018, date of publication November 1, 2018, date of current version November 30, 2018.

Digital Object Identifier 10.1109/ACCESS.2018.2879086

Single-Side-Scanning Surface Waveguide Leaky-Wave Antenna Using Spoof Surface Plasmon Excitation

SHANGKUN GE[1,2], (Student Member, IEEE), QINGFENG ZHANG[1], (Senior Member, IEEE), CHI-YUK CHIU[2], (Senior Member, IEEE), YIFAN CHEN[3], (Senior Member, IEEE), AND ROSS D. MURCH[2], (Fellow, IEEE)

[1]Department of Electronics and Electrical Engineering, Southern University of Science and Technology, Shenzhen 518055, China
[2]Department of Electronic and Computer Engineering, The Hong Kong University of Science and Technology, Hong Kong
[3]The University of Waikato, Hamilton 3216, New Zealand

Corresponding author: Qingfeng Zhang (zhang.qf@sustc.edu.cn)

This work was supported in part by the National Natural Science Foundation of China under Grant 61871207, in part by the Guangdong Natural Science Funds for Distinguished Young Scholar under Grant 2015A030306032, in part by the Talent Support Project of Guangdong under Grant 2016TQ03X839, and in part by the Shenzhen Science and Technology Innovation Committee Funds under Grant KQJSCX20160226193445, Grant JCYJ20160301113918121, and Grant JSGG20160427105120572.

ABSTRACT A surface waveguide (SWG) leaky-wave antenna featuring directional single-side beam scanning capability is presented. A novelty of the design is that transition design utilizes the spoof surface plasmon (SSP) as an intermedia to feed the SWG, which realizes an efficient SWG transition from the conventional coplanar waveguide. In addition, a novel spatial profile is modulated on the SWG to produce leaky-wave radiation. Because the transmission modes in SSP and SWG are similar, the transition exhibits low loss and broadband performance. Both the transition and the leaky-wave antenna are demonstrated using simulations and experiments. It is shown that the transition has an average loss of 0.61 dB across the frequency range 5–13 GHz, which is an improvement on other feeding techniques reported. It is also shown that the leaky-wave antenna produces a single-side scanning beam of 8.7 dB gain with an overall efficiency of 75%. The beam scans through a 43.5-degree range over the frequency 10–13 GHz.

INDEX TERMS Surface waveguides (SWG), spoof surface plasmon (SSP), leaky wave antenna, transition, beam scanning.

I. INTRODUCTION

Leaky wave antennas (LWA) have attracted extensive attention in recent decades, due to their advantages of being low profile and having a frequency-scanning property. LWA designs are realized using various structures including composite right/left handed lines [1], substrate integrated waveguides [2], magnetoelectric dipoles [3] and single-conductor lines [4], [5]. Among them, single-conductor LWAs are becoming popular due to their high radiation efficiency, low profile cross-section, and their ease of fabrication.

Two main categories of single-conductor transmission lines have been extensively investigated. The first is based on the spoof surface plasmon (SSP) [6] and the other is the surface waveguide (SWG) [7]–[9]. SSP mimicks surface plasmons (SPs) at optical regimes [10] and employs a corrugated surface to support a surface wave [6], [11]. SSP has been extensively studied and several transitions have been reported to convert a conventional transmission line (TL) feed to an SSP line [6], [12]. However, not many free parameters, except the corrugation depth, are available for controlling the dispersion characteristics of SSP lines. Typically, achieving a low cutoff requires a high corrugation depth and hence a broad line width. In contrast, SWG provides more flexibility in the control of its dispersion characteristics and this is achieved by changing the internal geometry of the SWG line without reconfiguring its line width. Therefore, SWG is a much more promising candidate for guiding surface waves. However, it is challenging to efficiently feed SWG. In previous studies, different methods have been explored and these include trapezoidal sheet [13], rectangular waveguides [8], and quasi-Yagi-Uda directional antennas [7]. These feeding techniques cannot realize high-efficiency mode conversion

and therefore an efficient feeding structure for SWG is still an open problem.

For single-conductor LWAs, single-layer SSP LWAs [14] are limited by the omnidirectional H-plane radiation patterns they produce. Two techniques were proposed to achieve single-side beam scanning capability. The first was to load large circular patches on one side of the SSP transmission line [5]. The other placed additional ground planes underneath the LWA with quarter-wavelength separation [15]. Both of these techniques result in a wider or thicker radiator. SWG LWA, featuring flexible control of dispersion and field profile, is a promising candidate to achieve single-side beam scanning.

In this paper, we propose a novel SWG LWA for single-side beam scanning. Unlike SSP LWAs [5], [15], it does not need addtional patches or increases thickness. In addition, we propose using SSPs as an intermedia for feeding SWG. Because the modes in SSP and SWG are similar, this SSP-based transition exhibits good mode conversion efficiency. Contributions of this work include: 1) overcoming the issues of double-side beam scanning in single-conductor LWAs by using a SWG LWA approach; 2) using SSP as an intermedia to efficiently feed SWG.

This paper is organized as follows. Sec. II reviews the principles of SWGs and SSP transmission lines. Sec. III provides a theoretical analysis of SSP-SWG transitions, followed by three different SWG TLs excited by our proposed transition. In Sec. IV, the experimental validation of our proposed SWG LWA is presented while a conclusion is provided in Sec. V.

II. SINGLE-CONDUCTOR LINE PRINCIPLES

A. SURFACE WAVEGUIDE

Surface waveguides (SWGs) are open-boundary structures supporting a tightly confined surface wave propagating with phase velocity less than that of light [16]. SWGs have been theoretically analyzed using an optics method [17] and a transmission line model [18]. Straight and curved SWGs have been constructed and validated [7], [13], showing that surface waves are tightly confined around SWGs. Based on these properties, SWGs are widely used for various microwave applications, such as beam shifters [19], phase shifters [20], [21], absorbers [22], [23] and leaky-wave antennas [24]–[26].

Realizations of SWGs include dielectric-coated wires [27], periodic dielectric waveguides [28], corrugated structures [29] and pin-bed structures [30]. Due to their straightforward fabrication and flexible design, planar periodic structures with subwavelength patterns are most commonly studied. The design patterns of the unit cell generally determine the properties of SWGs. By using different patterns, the surface waves can be polarized in a transverse electric (TE) mode, a transverse magnetic (TM) mode or a hybrid mode [8]. The unit cells can also be divided into ''scalar'' or ''tensor'' depending on whether their properties are dependent on directions [7]. Planar grids [31] and self-complementary geometries [32] are theoretically analyzed to investigate the relation between unit cells and supported surface waves.

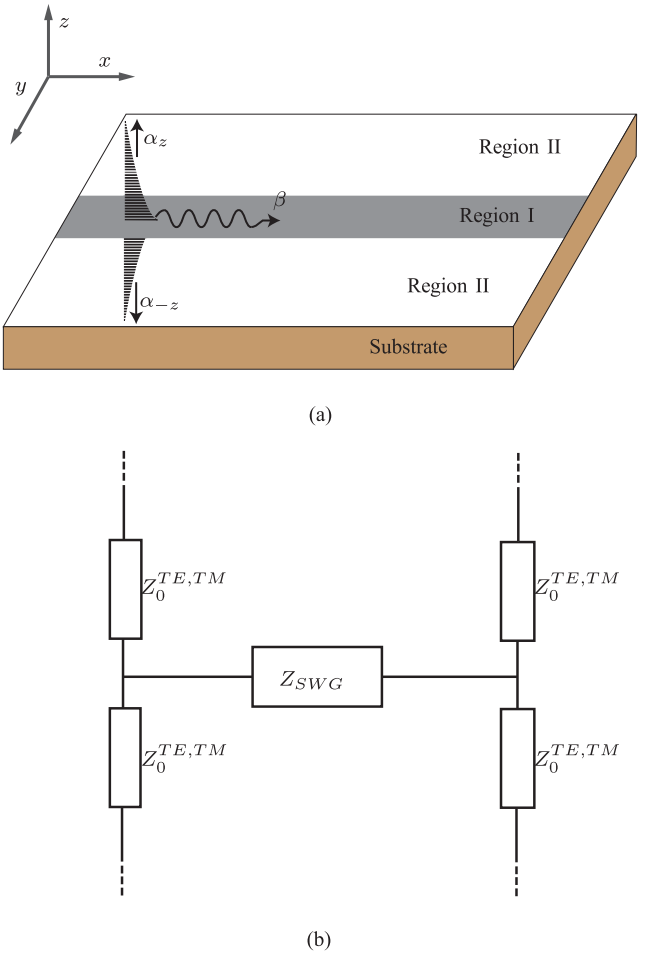

FIGURE 1. (a) Configuration and (b) transverse circuit model of SWG transmission line.

A model for a SWG is shown in Fig. 1(a), where region I is the surface waveguide with high surface wave impedance and region II is the substrate with low surface wave impedance. The wave along the SWG can be expressed as $e^{j\omega t}e^{-j\beta x}e^{-\alpha|z|}$ ($\beta > 0, \alpha > 0$), where β is the wave vector in the $+x$ direction and α is the attenuation constant along the $\pm z$ direction. The wave function manifests itself as a surface wave propagating along the $+x$ direction without any loss (in ideal case) and is exponentially decaying in the $-z$ or $+z$ directions. The wave vector and attenuation constant satisfy

$$k_0^2 = \beta^2 - \alpha^2, \tag{1}$$

where $k_0 = \omega/c$ is the wave vector in free-space.

In Fig. 1(a), the substrate does not have a ground and its depth is much smaller than the operational wavelength. Therefore, the SWG can be approximated as being suspended in free-space and the corresponding transverse equivalent circuit model is shown in Fig. 1(b). According to the transverse

resonance condition [33],

$$1/Z_0^{\mathrm{TM,TE}} + 1/Z_0^{\mathrm{TM,TE}} + 1/Z_{\mathrm{SWG}}^{\mathrm{TM,TE}} = 0 \tag{2}$$

where $Z_0^{\mathrm{TM,TE}}$ represents the TM or TE wave impedance in free-space, and $Z_{\mathrm{SWG}}^{\mathrm{TM,TE}}$ is the surface wave impedance of SWG,

$$Z_{\mathrm{SWG}}^{\mathrm{TM,TE}} = -\frac{Z_0^{\mathrm{TM,TE}}}{2}. \tag{3}$$

The TM and TE wave impedance is expressed by [34]

$$Z_0^{\mathrm{TM}} = -j\eta_0 \frac{\alpha}{k_0} = -j\eta_0 \sqrt{\frac{\beta^2}{k_0^2} - 1}, \tag{4}$$

$$Z_0^{\mathrm{TE}} = j\eta_0 \frac{k_0}{\alpha} = j\eta_0 \frac{1}{\sqrt{\frac{\beta^2}{k_0^2} - 1}}, \tag{5}$$

where η_0 is the characteristics impedance of free-space. By substituting (3) and (4) into (2), the surface impedance of SWG is computed as

$$Z_{\mathrm{SWG}}^{\mathrm{TM}} = -\frac{j\eta_0}{2} \sqrt{\frac{\beta^2}{k_0^2} - 1}, \tag{6}$$

$$Z_{\mathrm{SWG}}^{\mathrm{TE}} = \frac{j\eta_0}{2\sqrt{\frac{\beta^2}{k_0^2} - 1}}. \tag{7}$$

It is interesting to note from (6) and (7) that, for TM mode, a larger value of $|Z_{\mathrm{SWG}}^{\mathrm{TM}}|$ indicates a lower phase velocity, whereas, for TE mode, a larger value of $|Z_{\mathrm{SWG}}^{\mathrm{TE}}|$ corresponds to a higher phase velocity. One also finds that the TM-mode SWG has inductive surface impedance and TE-mode SWG has capacitive surface impedance.

The surface wave impedance is an important parameter to describe the property of light-matter interaction at the surface of two media. The characteristic impedance of the propagating waves in x direction, $Z_x = \eta_0\beta/k_0$, is uniquely determined by the surface impedance according to (6) and (7). Therefore, by finding the surface wave impedance, one is also able to check the impedance matching between two SWGs connected together. A low reflection coefficient typically requires two equal characteristic impedances and hence two equal surface impedances.

B. SSP TRANSMISSION LINE

SSP mimick surface plasmons (SPs) at optical regimes [10] and employ a corrugated surface to support a surface wave [6], [11]. In order to connect SSP circuits to traditional microwave circuits, the CPW-SSP (Coplanar Waveguide-SSP) transition has been proposed [6], [12]. SSPs are employed in many microwave applications including slow-wave transmission line [35], frequency splitters [36], couplers [37], and filters [38], [39].

Fig. 2 shows a typical SSP transmission line based on H-shape unit cells. It is printed on a substrate without a ground and consists of two main parts including a transition part and SSP line part. The transition part can achieve high-efficiency and broadband conversion from traditional CPW modes to SSP mode by using a smoothly flared ground plane. From the electric and magnetic distribution of Fig. 2, one finds that the dominant SSP mode belongs to a TM-mode surface wave. Strictly speaking, SSP belongs to a special case of SWGs but here we still use the terminology "SSP" to help readers easily connect it with other related works.

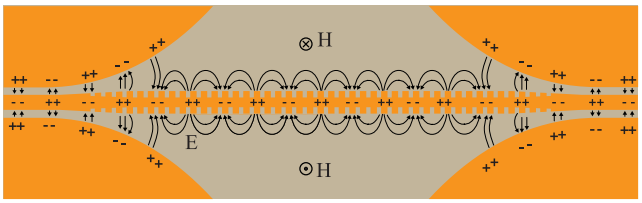

FIGURE 2. Electric and magnetic field distribution of SSP transmission line.

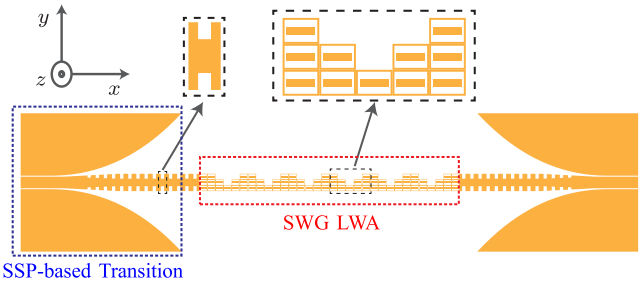

FIGURE 3. Configuration of the proposed SWG LWA including the SSP-based transition.

TABLE 1. Dimensions for CPW-SSP Transition (Unit: mm).

a	b	s	l	l_1	l_2
4	21.65	0.35	55.78	15	18.67

III. GEOMETRY AND DESIGN OF THE SSP-FED SWG LWA

Fig. 3 illustrates the geometry of our proposed single-side-scanning SWG LWA including SSP-based transition. The SSP-based transition includes a CPW (coplanar waveguide) to SSP transition and a SSP to SWG connection. SSPs work as an intermedia to connect two different modes. The SWG LWA is realized by periodically modulating the profile of the SWG. Both the SSP-based transition and SWG LWA are described in the following sections where dimensions are also provided.

A. SSP-BASED TRANSITION

To demonstrate the SSP-based transition, we use a SWG connected by two SSP-based transitions, as shown in Fig. 4. The whole transition includes two steps, namely, CPW to SSP and SSP to SWG. We excite the SSP using a CPW-SSP transition [6], [12]. The dimensions of the SSP-based transition are listed in Tab. 1.

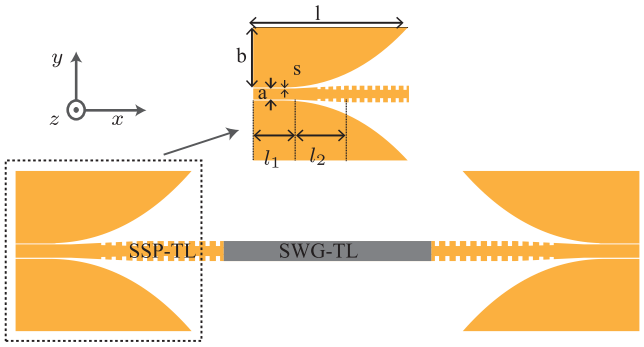

FIGURE 4. The schematic illustration for transition from CPW to SSP and further to SWG.

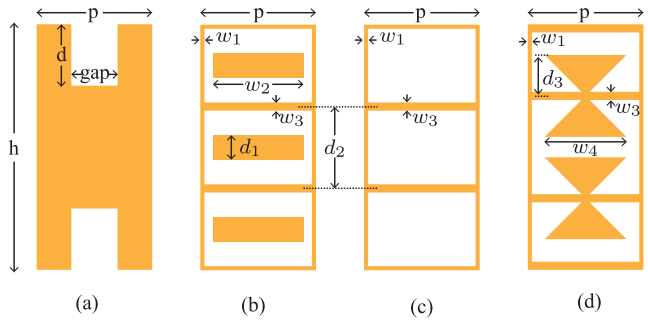

FIGURE 5. Unit cells of the SSP. (a) H-shape SSP unit cell; (b) Unit Cell 1, (c) Unit Cell 2, and (d) Unit Cell 3 of SWG TL. The the dimensions are respectively as follows: $h = 6$ mm, $p = 2.825$ mm, $gap = 1.13$ mm, $d = 1.5$ mm, $d_1 = 0.6$ mm, $d_2 = 2$ mm, $d_3 = 1$ mm, $w_1 = 0.1$ mm, $w_2 = 2.2125$ mm, $w_3 = 0.2$ mm, $w_4 = 2$ mm.

To better demonstrate the performance of this SSP-based transition, we consider three SWGs. The unit cells of the SSP and the three SWGs are shown in Fig. 5. All of these unit cells are fixed with the same width, h, but different inner configurations. The patterns are printed on a substrate without a ground (Rogers 4003C of thickness 1.52 mm). For the unit cell design, a uniform width is employed to avoid radiation loss. And the inner configurations determine the cut-off frequency of dispersion curves. Fig. 6 shows the dispersion curves for the unit cells in Fig. 5. Note that, the three SWG unit cells exhibit different dispersion curves and different cutoff frequencies. Therefore we can reconfigure the cutoff frequency and dispersion curves without resorting to changing the line width (h) and this is one important benefit of SWG.

In Fig. 7 we compare the surface wave impedances of SSP and the three SWGs and observe that, the surface wave impedances of the three SWGs are almost the same below 14 GHz. Therefore, it is possible to match the three SWGs using one transition only. The surface wave impedance of SSP is slightly larger than those of SWGs, which, to be validated later by simulated and measured scattering parameters, leads a small reflections within an acceptable level. Since SSP and SWGs change the surface impedances in a similar manner below the cutoff frequency, SSP-based transition provides broadband matching.

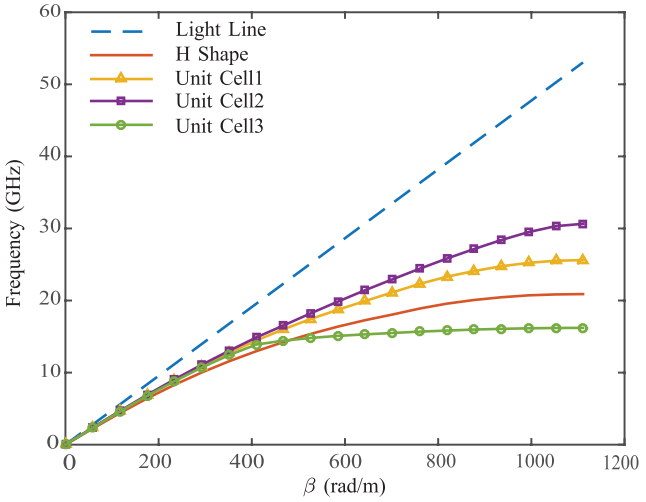

FIGURE 6. Dispersion curves of the SSP unit and three different SWG units in Fig. 5.

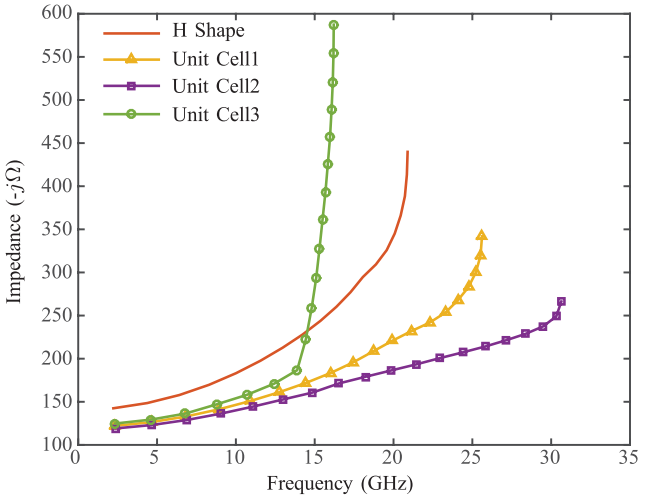

FIGURE 7. Surface impedances of SSP and SWGs.

B. SWG LWA

From Fig. 6 we can observe that the dispersion curves of the SWGs are all below that for free space. Therefore, the dominant mode for a SWG is a slow-wave mode that does not radiate into free space. For leaky-wave radiation to occur, it needs an additional phase (or momentum) and this is typically realized by periodically modulating the profile of slow-wave structures. This leads to an infinite set of space harmonics with

$$\beta_n = \beta_0 + \frac{2\pi n}{p}, \tag{8}$$

where β_n and β_0 are the wavenumbers of the n^{th} space harmonic and fundamental mode, respectively and p is the modulation period. By carefully selecting the modulation period, one is able to let $n = -1$ so that space harmonics fall into the fast-wave region, i.e. $-k_0 < \beta_{-1} < k_0$, and enables radiation.

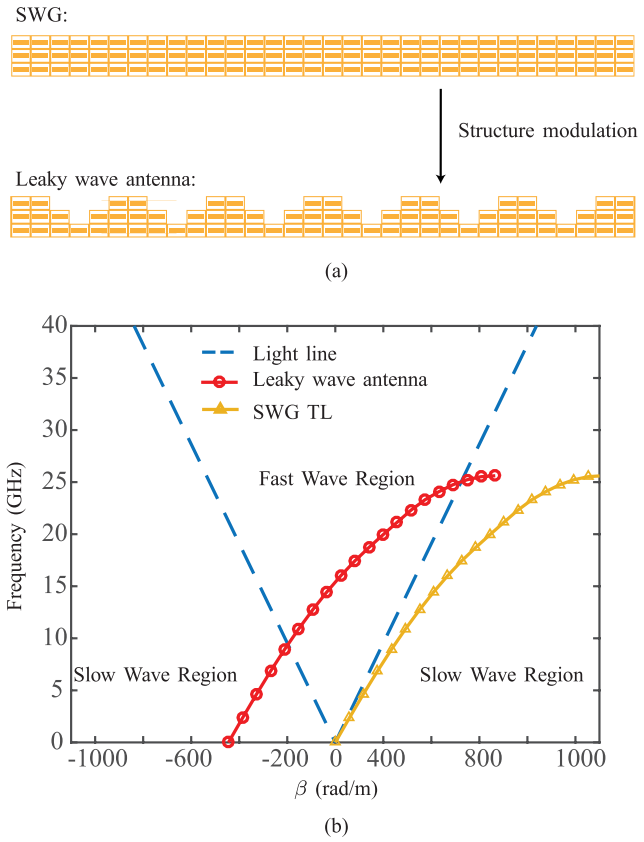

FIGURE 8. (a) Profile modulation scheme for the SWG LWA; (b) Dispersion curves of $n = -1$ space harmonics and the original SWG.

As an example we use the unit cell in Fig. 5(b) and the profile modulation scheme shown in Fig. 8(a). If the modulated sections of the SWG line are periodically removed from its upper side, we can produce leaky-wave radiation focused in the upper direction leading to a single-side directional beam. Note that, this single sided profile modulation not only provides a single-sided beam, but also maintains a compact and low-profile configuration. In this design, the modulation period is set to $m = 14.125$ mm and the resultant dispersion curve shift is illustrated in Fig. 8(b). Such a profile modulation approach was also studied in SSP leaky-wave antenna [14], which however has an omnidirectional radiation beam in the transverse plane.

IV. EXPERIMENTAL VALIDATION

A. SSP-BASED TRANSITION

In order to demonstrate the performance of the proposed SSP-based transition, we apply it to the three SWGs shown in Fig. 5. The results are shown in Fig. 9 where the SWG transmission lines were simulated in CST Microwave Studio and fabricated on a 1.52 mm thick Rogers 4003C substrate with $\epsilon_r = 3.38$. Taking the SWG TL based on unit cell 1 for example, Fig. 10(a) provides the simulated electric field distribution at 10 GHz on the x-y plane and x-z plane and Fig. 10(b) provides results for the simulated magnetic field distribution on the transverse plane (y-z plane). The electric

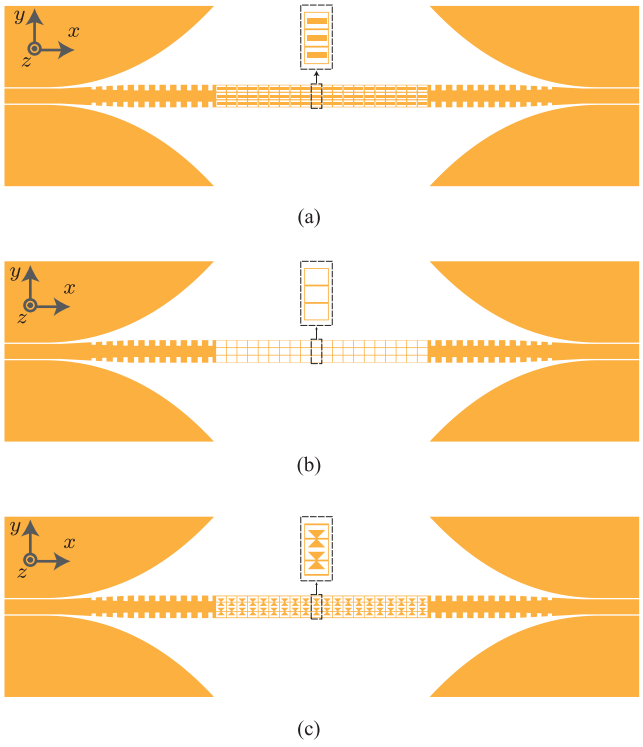

FIGURE 9. Three SWG TLs, based on (a) unit cell 1, (b) unit cell 2, and (c) unit cell 3, all fed by SSP-SWG transition.

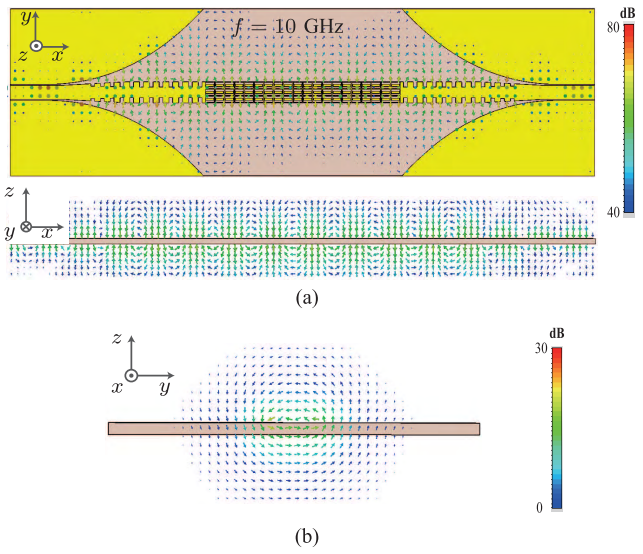

FIGURE 10. (a) Electric field distribution on $x - y$ plane and $x - z$ plane. (b) Magnetic field distribution on $y - z$ plane.

field smoothly transits at the interface between the SSP structures and SWGs, and the surface waves propagate along SWG in the form of a TM mode, which accords with our analysis.

The fabricated prototypes of the three samples are shown in the insets of Fig. 11. The scattering parameters are measured by a Vector Network Analyzer (VNA) and Figs. 11(a), (b) and (c) show the simulated and measured scattering parameters of the three SWGs with SSP-based

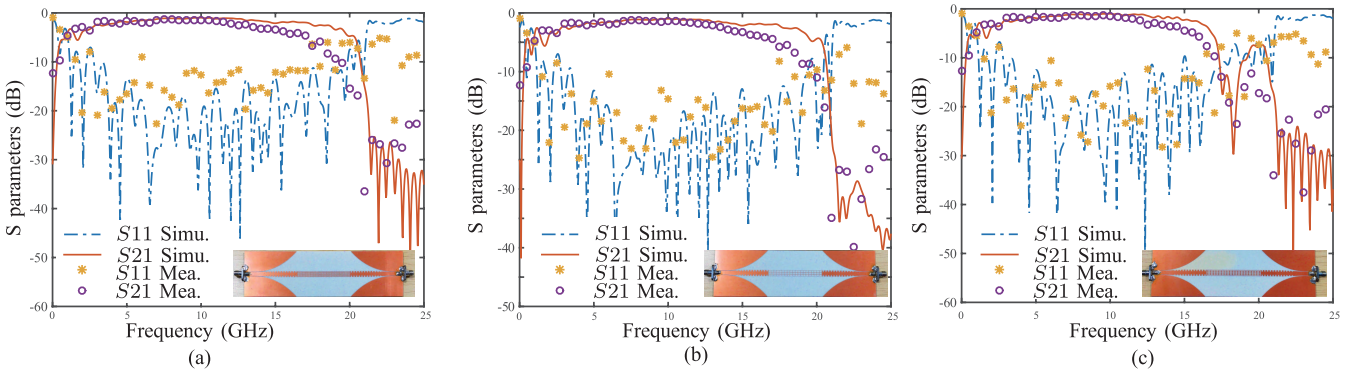

FIGURE 11. Simulated and measured scattering parameters of three SWG TLs: (a) unit cell 1, (b) unit cell 2, (c) unit cell 3.

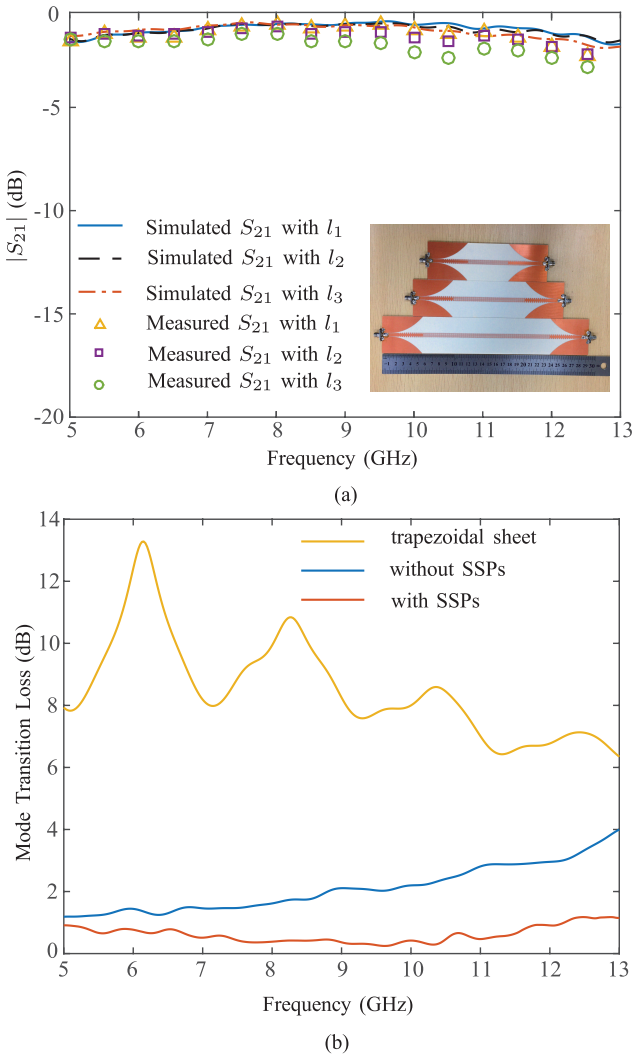

FIGURE 12. (a) Simulated and measured S_{21} of three different length SWG TLs based on unit cell1; (b) Extracted mode transition loss comparison among three transition designs.

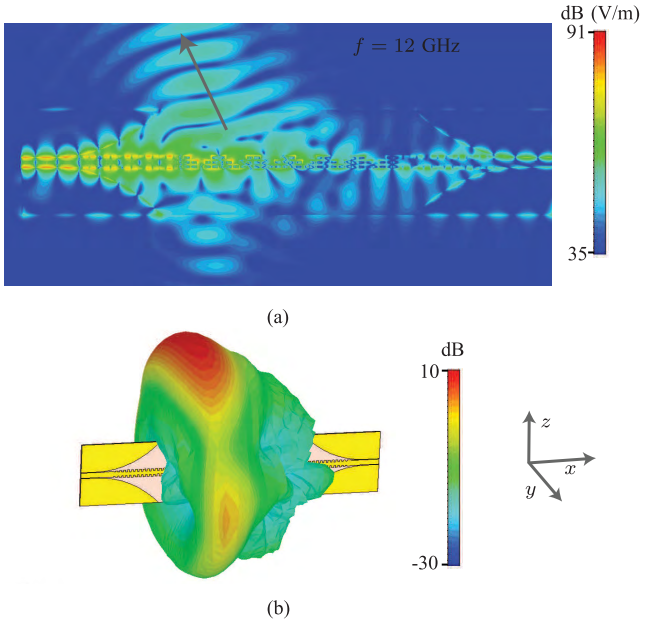

FIGURE 13. (a) Electric field distribution and (b) 3D far field pattern of SWG LWA at 12 GHz.

transitions, respectively. Since SSP and SWGs are connected in series, the overall cut-off frequency is determined by the smaller of the two cutoff frequencies. In Fig. 6, Unit Cell 3 has a smaller cutoff frequency (16 GHz) than SSP (20.5 GHz) and as a result, the simulated and measured $|S_{21}|$ go down sharply around 16 GHz, as shown in Fig. 11(c). In contrast, Unit Cell 1 and Unit Cell 2 have higher cutoff frequencies than SSP, which results in their transmissions being attenuated around 20.5 GHz, as shown in Fig. 11(a) and 11(b). The reflection coefficients $|S_{11}|$ of the three SWGs are below -10 dB across a broad frequency range. The measured transmission responses closely follow the simulated result below 13 GHz and deviate above 13 GHz. This difference between the measured and simulated responses above 13 GHz is mainly attributed to the loss of the SMA, which practically works well only below 13 GHz. Above 13 GHz, the SMA loss plays the most significant role. And in simulation, metal and substrate are ideally lossless, which also leads to a little difference between simulated and measured results.

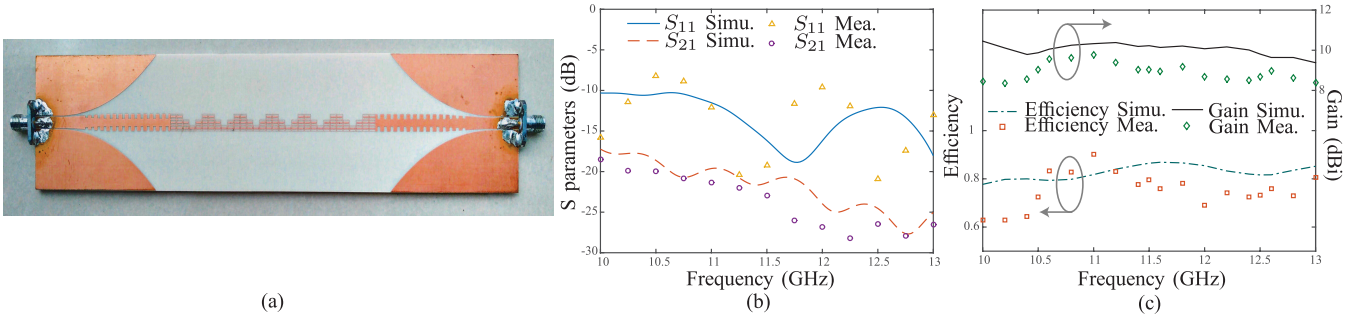

FIGURE 14. (a) Fabricated prototype, (b) scattering parameters, and (c) gain and efficiency of the proposed SWG LWA.

Additionally, since all the single-conductor lines have lower cutoff frequencies, the transmission drops when it is close to the cutoff frequency. Therefore, we consider the frequency range 5-13 GHz in this design.

To determine the loss of CPW-SWG transition, we fabricate and measure the SWG transmission lines with three different lengths ($l_1 = 169$ mm, $l_2 = 214.2$ mm, $l_3 = 293.3$ mm), as shown in Fig. 12(a). The total loss consists of two parts consisting of a transition loss and a SWG loss. Since the transition loss is independent of the length of the SWG, it is possible to calculate the SWG loss by comparing two samples with different lengths. Fig. 12(b) shows the extracted SWG loss by averaging the differences between every two samples in Fig. 12(a). Upon obtaining SWG loss per unit length, the mode transition loss is readily calculated by removing the SWG loss from the overall loss. In Fig. 12(b), the mode transition loss is found to be between 0.2-1.2 dB within 5-13 GHz. Considering that the whole mode transition includes a CPW-SSP transition and a SSP-CPW transition, the pure transition part from SSP to SWG should have a much smaller loss than its average value 0.61 dB. In addition, our transition performance is compared with the designs without SSPs and trapezoidal sheet [13]. Here, all transition designs use the same length for a fair comparison. Note that the conversion loss of trapezoidal sheet is significantly larger than the other two designs. And when SWG is directly excited by the tapered CPW without SSPs as the intermedia, the transition loss from CPW to SWG is between 1.16-2.64 dB within 5-13 GHz. In contrast, the transition loss with SSPs is reduced by 1 dB within 5-13 GHz. This well demonstrates the benefit of the proposed transition design.

B. SWG LWA

We use 10-13 GHz as the frequency range for experimental validation and it was determined by noting that the leaky mode enters the fast wave region after 9 GHz (see Fig. 8(b)) and that the SMA connector performs well only below 13 GHz.

Using this range the SWG LWA is simulated in CST Microwave Studio and Fig. 13(a) shows the x-z plane electric field distribution at 12 GHz. At the transition region, the energy steadily flows from the CPW to the SWG and no leaky wave is produced. When it comes into the modulated SWG region, energy partly leaks from the SWG. After going through several modulated units, most power has leaked out and little power is received by port 2. The direction of leaky wave flow is towards the upward area, which corresponds with the profile modulation side. Fig. 13(b) shows the simulated 3D radiation pattern at 12 GHz. The main beam is directional and radiates towards the upper side (or positive z axis).

The fabricated prototype of this SWG LWA is shown in Fig. 14(a) and the measured scattering parameters are shown in Fig. 14(b). Overally these results agree with each other in a reasonable manner. The difference between simulation and measurement is partly attributed to the SMA connector that is not considered in simulation, and is partly due to the fabrication tolerance and dielectric tolerance. Within the frequency range 10-13 GHz, S_{11} is almost below -10 dB, indicating that the impedance matching is good and the energy goes into SWG LWA with minimal return loss by using the SSP-SWG transition. The transmission coefficient S_{21} is below -15 dB, indicating that most energy has leaked out and little energy is received by port 2. Therefore, the received port in our LWA design doesn't affect the radiation pattern and can be removed. In order to illustrate the design principle clearly, the second port is retained in simulation and experiment.

The radiation patterns were measured in an anechoic chamber and the measured gain and efficiency are shown in Fig. 14(c). The average measured gain is about 8.7 dB and the gain variation is about 1.36 dB over the whole frequency band. The gains are consistent over the entire frequency band. The measured gain is on average 1 dB smaller than that simulated, which may be attributed to the fact that the practical materials (including substrate and copper) are more lossy than the simulated model. For the main beams at different operating frequencies, the levels of cross polarizations are all less than -22.7 dB with respect to the co-polarizations. The average measured efficiency is about 75%. The radiation patterns in x-z and y-z planes are displayed in Fig. 15. The simulated and measured results are compared at 10, 11, 12, 13 GHz, respectively. Both results agree well with each other. In x-z plane, the measured main beam steers from $\theta = -51°$ to $-7.5°$ as the operating frequency increases from 10 GHz to 13 GHz. The total scanning angle is about 43.5°. The main beams radiate in the backward direction and corresponds

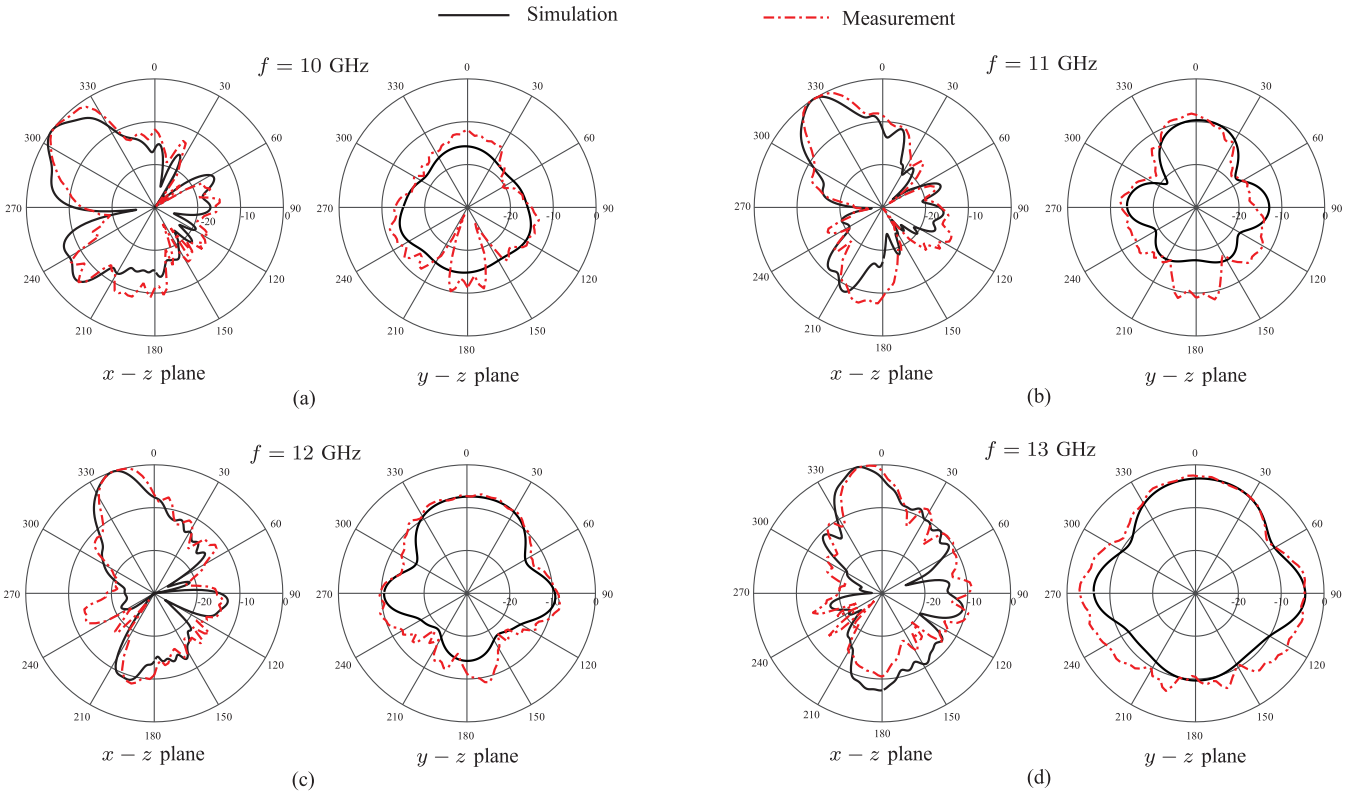

FIGURE 15. Radiation patterns of x-z plane and y-z plane at (a) 10 GHz, (b) 11 GHz, (c) 12 GHz, and (d) 13 GHz.

with β_{-1} being less than zero within the frequency band 10-13 GHz according to Fig. 8(b). In y-z plane, the beam does not scan as the frequency changes and mainly radiates into the positive z direction. In addition, the sidelobe enhances in broadside direction due to that β_{-1} is approaching to zero, which will result in more broadside radiation. Therefore, the main beam is unidirectional and only scans the upper half space in x-z plane, which well demonstrates the functionality of single-side scanning.

V. CONCLUSION

In this paper, a novel single-side-scanning SWG LWA is presented. Due to the flexibility of the SWG, the whole design is very compact and only uses a single-layer conductor. In addition, a SSP-based transition is provided to efficiently excite SWG. The mode transition loss is less than 0.61 dB within 5-13 GHz. Fed by the SSP transition, the proposed SWG LWA obtains a gain of 8.7 dBi and overall efficiency of 75%. The antenna can also achieve 43.5° scanning. An important result is that the proposed SSP-SWG transition allows SWG to efficiently connect with the proposed LWA. In addition it could also be used with traditional microwave circuits greatly benefiting the integration of SWG circuits.

REFERENCES

[1] C. Caloz, T. Itoh, and A. Rennings, "CRLH metamaterial leaky-wave and resonant antennas," *IEEE Antennas Propag. Mag.*, vol. 50, no. 5, pp. 25–39, Oct. 2008.

[2] J. Liu, D. R. Jackson, and Y. Long, "Substrate integrated waveguide (SIW) leaky-wave antenna with transverse slots," *IEEE Trans. Antennas Propag.*, vol. 60, no. 1, pp. 20–29, Jan. 2012.

[3] K.-M. Mak, K.-K. So, H.-W. Lai, and K.-M. Luk, "A magnetoelectric dipole leaky-wave antenna for millimeter-wave application," *IEEE Trans. Antennas Propag.*, vol. 65, no. 12, pp. 6395–6402, Dec. 2017.

[4] A. Kianinejad, Z. N. Chen, and C.-W. Qiu, "A single-layered spoof-plasmon-mode leaky wave antenna with consistent gain," *IEEE Trans. Antennas Propag.*, vol. 65, no. 2, pp. 681–687, Feb. 2017.

[5] J. Y. Yin *et al.*, "Frequency-controlled broad-angle beam scanning of patch array fed by spoof surface plasmon polaritons," *IEEE Trans. Antennas Propag.*, vol. 64, no. 12, pp. 5181–5189, Dec. 2016.

[6] A. Kianinejad, Z. N. Chen, and C.-W. Qiu, "Design and modeling of spoof surface plasmon modes-based microwave slow-wave transmission line," *IEEE Trans. Microw. Theory Techn.*, vol. 63, no. 6, pp. 1817–1825, Jun. 2015.

[7] D. J. Gregoire and A. V. Kabakian, "Surface-wave waveguides," *IEEE Antennas Wireless Propag. Lett.*, vol. 10, pp. 1512–1515, 2011.

[8] M. Li, S. Xiao, J. Long, and D. F. Sievenpiper, "Surface waveguides supporting both TM mode and TE mode with the same phase velocity," *IEEE Trans. Antennas Propag.*, vol. 64, no. 9, pp. 3811–3819, Sep. 2016.

[9] B. H. Fong, J. S. Colburn, J. J. Ottusch, J. L. Visher, and D. F. Sievenpiper, "Scalar and tensor holographic artificial impedance surfaces," *IEEE Trans. Antennas Propag.*, vol. 58, no. 10, pp. 3212–3221, Oct. 2010.

[10] W. L. Barnes, A. Dereux, and T. W. Ebbesen, "Surface plasmon subwavelength optics," *Nature*, vol. 424, no. 6950, pp. 824–830, 2003.

[11] J. B. Pendry, L. Martín-Moreno, and F. J. Garcia-Vidal, "Mimicking surface plasmons with structured surfaces," *Science*, vol. 305, pp. 847–848, Aug. 2004.

[12] H. F. Ma, X. Shen, Q. Cheng, W. X. Jiang, and T. J. Cui, "Broadband and high-efficiency conversion from guided waves to spoof surface plasmon polaritons," *Laser Photon. Rev.*, vol. 8, no. 1, pp. 146–151, 2014.

[13] R. G. Quarfoth and D. F. Sievenpiper, "Nonscattering waveguides based on tensor impedance surfaces," *IEEE Trans. Antennas Propag.*, vol. 63, no. 4, pp. 1746–1755, Apr. 2015.

[14] G. S. Kong, H. F. Ma, B. G. Cai, and T. J. Cui, "Continuous leaky-wave scanning using periodically modulated spoof plasmonic waveguide," *Sci. Rep.*, vol. 6, Jul. 2016, Art. no. 29600.
[15] Q. Zhang, Q. Zhang, and Y. Chen. (2017). "Spoof surface plasmon polariton leaky-wave antennas using periodically loaded patches above PEC and AMC ground planes." [Online]. Available: https://arxiv.org/abs/1705.01098
[16] R. E. Collin, *Field Theory of Guided Waves*. New York, NY, USA: McGraw-Hill, 1960.
[17] R. Quarfoth and D. Sievenpiper, "Artificial tensor impedance surface waveguides," *IEEE Trans. Antennas Propag.*, vol. 61, no. 7, pp. 3597–3606, Jul. 2013.
[18] A. M. Patel and A. Grbic, "Effective surface impedance of a printed-circuit tensor impedance surface (PCTIS)," *IEEE Trans. Microw. Theory Techn.*, vol. 61, no. 4, pp. 1403–1413, Apr. 2013.
[19] R. Quarfoth and D. Sievenpiper, "Surface wave scattering reduction using beam shifters," *IEEE Antenna Wireless Propag. Lett.*, vol. 13, pp. 963–966, 2014.
[20] J. A. Higgins, H. Xin, A. Sailer, and M. Rosker, "Ka-band waveguide phase shifter using tunable electromagnetic crystal sidewalls," *IEEE Trans. Microw. Theory Techn.*, vol. 51, no. 4, pp. 1281–1288, Apr. 2003.
[21] D. Chicherin, S. Dudorov, D. Lioubtchenko, V. Ovchinnikov, S. Tretyakov, and A. V. Räisänen, "MEMS-based high-impedance surfaces for millimeter and submillimeter wave applications," *Microw. Opt. Technol. Lett.*, vol. 48, no. 12, pp. 2570–2573, 2006.
[22] Q. Gao, Y. Yin, D.-B. Yan, and N.-C. Yuan, "A novel radar-absorbing-material based on EBG structure," *Microw. Opt. Technol. Lett.*, vol. 47, no. 3, pp. 228–230, 2005.
[23] H. Wakatsuchi, S. Kim, J. J. Rushton, and D. F. Sievenpiper, "Waveform-dependent absorbing metasurfaces," *Phys. Rev. Lett.*, vol. 111, no. 24, p. 245501, Dec. 2013.
[24] A. M. Patel and A. Grbic, "A printed leaky-wave antenna based on a sinusoidally-modulated reactance surface," *IEEE Trans. Antennas Propag.*, vol. 59, no. 6, pp. 2087–2096, Jun. 2011.
[25] G. Minatti, F. Caminita, M. Casaletti, and S. Maci, "Spiral leaky-wave antennas based on modulated surface impedance," *IEEE Trans. Antennas Propag.*, vol. 59, no. 12, pp. 4436–4444, Dec. 2011.
[26] S. K. Podilchak, L. Matekovits, A. P. Freundorfer, Y. M. M. Antar, and M. Orefice, "Controlled leaky-wave radiation from a planar configuration of width-modulated microstrip lines," *IEEE Trans. Antennas Propag.*, vol. 61, no. 10, pp. 4957–4972, Oct. 2013.
[27] G. Goubau, "Single-conductor surface-wave transmission lines," *Proc. IRE*, vol. 39, no. 6, pp. 619–624, Jun. 1951.
[28] S. T. Peng, T. Tamir, and H. L. Bertoni, "Theory of periodic dielect waveguides," *IEEE Trans. Microw. Theory Techn.*, vol. MTT-23, no. 1, pp. 123–133, Jan. 1975.
[29] W. Rotman, "A study of single-surface corrugated guides," *Proc. IRE*, vol. 39, no. 8, pp. 952–959, Aug. 1951.
[30] R. J. King, D. V. Thiel, and K. Park, "The synthesis of surface reactance using an artificial dielectric," *IEEE Trans. Antennas Propag.*, vol. AP-31, no. 3, pp. 471–476, May 1983.
[31] O. Luukkonen *et al.*, "Simple and accurate analytical model of planar grids and high-impedance surfaces comprising metal strips or patches," *IEEE Trans. Antennas Propag.*, vol. 56, no. 6, pp. 1624–1632, Jun. 2008.
[32] D. González-Ovejero, E. Martini, and S. Maci, "Surface waves supported by metasurfaces with self-complementary geometries," *IEEE Trans. Antennas Propag.*, vol. 63, no. 1, pp. 250–260, Jan. 2015.
[33] R. Sorrentino and M. Mongiardo, "Transverse resonance techniques," *Encyclopedia RF Microw. Eng.*, Apr. 2005.
[34] R. F. Harrington, *Time-Harmonic Electromagnetic Fields*. New York, NY, USA: McGraw-Hill, 1961.
[35] A. Kianinejad, Z. N. Chen, and C.-W. Qiu, "Low-loss spoof surface plasmon slow-wave transmission lines with compact transition and high isolation," *IEEE Trans. Microw. Theory Techn.*, vol. 64, no. 10, pp. 3078–3086, Oct. 2016.
[36] X. Gao *et al.*, "Ultrathin dual-band surface plasmonic polariton waveguide and frequency splitter in microwave frequencies," *Appl. Phys. Lett.*, vol. 102, no. 15, p. 151912, 2013.
[37] X. Liu, Y. Feng, K. Chen, B. Zhu, J. Zhao, and T. Jiang, "Planar surface plasmonic waveguide devices based on symmetric corrugated thin film structures," *Opt. Express*, vol. 22, no. 17, pp. 20107–20116, 2014.
[38] X. Gao, L. Zhou, Z. Liao, H. F. Ma, and T. J. Cui, "An ultra-wideband surface plasmonic filter in microwave frequency," *Appl. Phys. Lett.*, vol. 104, no. 19, p. 191603, 2014.
[39] X.-L. Tang, Q. Zhang, S. Hu, A. Kandwal, T. Guo, and Y. Chen, "Capacitor-loaded spoof surface plasmon for flexible dispersion control and high-selectivity filtering," *IEEE Microw. Wireless Compon. Lett.*, vol. 27, no. 9, pp. 806–808, Sep. 2017.

SHANGKUN GE (S'17) received the bachelor's degree in communication engineering from the Southern University of Science and Technology, Shenzhen, China, in 2016. He is currently pursuing the joint Ph.D. degree with the Southern University of Science and Technology, and The Hong Kong University of Science and Technology, Hong Kong. His research interests include leaky wave antenna, and surface wave theory and applications.

QINGFENG ZHANG (S'07–M'11–SM'15) received the B.E. degree in electrical engineering from the University of Science and Technology of China, Hefei, China, in 2007, and the Ph.D. degree in electrical engineering from Nanyang Technological University, Singapore, in 2011. From 2011 to 2013, he was with the Poly-Grames Research Center, École Polytechnique de Montréal, Montreal, QC, Canada, as a Post-Doctoral Fellow. Since 2013, he has been with the Southern University of Science and Technology, Shenzhen, China, as an Assistant Professor. His current research interests include emerging novel electromagnetics technologies and multidispliniary topics. He was a recipient of the Shenzhen Overseas High-Caliber Personnel in 2014, the Guangdong Natural Science Funds for Distinguished Young Scholar in 2015, the Shenzhen Nanshan Piloting Talents in 2016, and the Guangdong Special Support Program for Top-Notch Young Talents in 2017. He was the Publication Chair at the IEEE International Conference on Communication Systems in 2016. He was a Lead Guest Editor of the *International Journal of Antennas and Propagation* from 2014 to 2015.

CHI-YUK CHIU (M'05–SM'12) received the B.Eng., M.Eng., and Ph.D. degrees in electronic engineering from the City University of Hong Kong, Hong Kong, in 2001, 2001, and 2005, respectively. He joined the Department of Electronic and Computer Engineering (ECE), The Hong Kong University of Science and Technology (HKUST), Hong Kong, as a Research Associate in 2005. He was with Sony Mobile Communications, Beijing, China, as a Senior Antenna Engineer, in 2011. Since 2015, he has been with HKUST, where he is currently a Research Assistant Professor with the Department of ECE. He has authored 54 papers and one book chapter and holds five patents (two pending) related to antenna technology. His current research interests include the design and analysis of small antennas, MIMO antennas, MIMO measurements, and energy harvesting. He is a member of the IEEE Antennas and Propagation Society Education Committee. He is also an active reviewer for several journals, including the IEEE Transactions on Antennas and Propagation and the IEEE Antennas and Wireless Propagation Letters.

YIFAN CHEN (M'06–SM'14) received the B.Eng. (Hons.) and Ph.D. degrees in electrical and electronic engineering from Nanyang Technological University in 2002 and 2006, respectively. From 2005 to 2007, he was a Project Officer and then a Research Fellow with the Singapore-University of Washington Alliance in bioengineering, supported by the Singapore Agency for Science, Technology and Research, Nanyang Technological University, Singapore, and the University of Washington, Seattle, USA. From 2007 to 2012, he was a Lecturer and then a Senior Lecturer with the University of Greenwich and Newcastle University, U.K. From 2012 to 2016, he was a Professor and the Head of the Department of Electrical and Electronic Engineering, Southern University of Science and Technology, Shenzhen, China, appointed through the Recruitment Program of Global Experts—the Thousand Talents Plan. In 2013, he was a Visiting Professor with the Singapore University of Technology and Design, Singapore. He is currently with The University of Waikato, Hamilton, New Zealand, as a Professor of Engineering and the Associate Dean External Engagement of the Faculty of Science and Engineering and the Faculty of Computing and Mathematical Sciences, The University of Waikato.

ROSS D. MURCH (M'84–SM'98–F'09) received the bachelor's and Ph.D. degrees in electrical and electronic engineering from the University of Canterbury, Christchurch, New Zealand. He was the Department Head of The Hong Kong University of Science and Technology, Hong Kong, from 2009 to 2015, where he is currently a Chair Professor with the Department of Electronic and Computer Engineering. He has authored or co-authored over 200 publications and 20 patents on wireless communication systems and antennas and these have attracted over 12,000 citations in his research fields. His current research interests include the Internet-of-Things, underwater acoustics, and antenna design and his unique expertise lies in his combination of knowledge from both wireless communication systems and electromagnetic areas. He received several awards, including the Computer Simulation Technology University Publication Award in 2015. He has served the IEEE in various positions, including an Area Editor, a Technical Program Chair, a Distinguished Lecturer, and a fellow of Evaluation Committee.